The Orbital Dynamics Environment of 433 Eros: A Case Study for Future Asteroid Missions

D. J. Scheeres,[1] J. K. Miller,[2] and D. K. Yeomans[2]

The Near-Earth Asteroid Rendezvous (NEAR)–Shoemaker mission was a milestone in that it represented the practical navigation of a spacecraft in the most severely perturbed orbital environment (relative to the standard two-body problem) ever experienced by a spacecraft. Furthermore, all future asteroid orbital missions will encounter environments similar, in some way, to the environment encountered by NEAR at Eros. Thus, it is of interest to discuss the orbital dynamics that the NEAR-Shoemaker spacecraft was subject to at Eros. This article first provides a brief review of the measured force and model parameters of Eros. Next, an evaluation of the resulting orbital dynamics environment in the vicinity of Eros is made using these estimated values. The Eros dynamical environment is discussed in the region relatively far from the asteroid, where solar effects are the dominant perturbation, and in the region close to the asteroid, where the gravity field and rotation of Eros are most important. In particular, we give limits for stable motion about Eros and provide analytical descriptions of the dynamical environment found there. Many of the methods discussed and introduced in this article can be used for future asteroid missions as well.

I. Introduction

While the force environment at asteroids is unique for each separate body, the analysis and evaluation of these environments can be formulated in a general manner that can be equally applied to each new situation. Thus, in this article we consider a somewhat detailed discussion of the dynamical environment about Eros, formulated in such a fashion as to be applicable to most asteroids. Specifically, we consider the dynamical environment far from and close to an asteroid, where strong perturbation forces exist. Far from an asteroid, the perturbations arise from solar radiation pressure and solar tidal forces. Close to an asteroid, the perturbations arise from the gravity field and rotation state of the body. The one case that is not explicitly covered in the current analysis is when the solar radiation pressure and asteroid gravity-field spheres of influence overlap. This situation can lead to interesting interactions between these competing perturbations and is an area of practical interest as future missions to near-Earth asteroids likely would fall into this regime.

[1] Department of Aerospace Engineering, University of Michigan, Ann Arbor.

[2] Navigation and Mission Design Section.

The research described in this publication was carried out by the Jet Propulsion Laboratory, California Institute of Technology, under a contract with the National Aeronautics and Space Administration.

II. Navigation Model of Eros Environment

During the course of its mission, the Near-Earth Asteroid Rendezvous (NEAR) spacecraft was used as a probe to determine the force environment about Eros. This determination arose naturally from the navigation of the spacecraft, as precision estimates of the force environment are needed to predict, guide, and reconstruct the spacecraft trajectory [7]. There was also a strong scientific interest in the Eros force environment, as its gravity field and shape can be used to infer the distribution of mass density within the body [17].

The estimation of the asteroid's force parameters involved the simultaneous processing of radio metric Doppler data and optical images of the asteroid's surface. Altimetry measurements from the spacecraft to the asteroid were used in a post-processing mode to determine the asteroid's shape. A complete and detailed description of the determination of the shape, gravity, and rotational state of Eros is provided in Miller et al. [8].

A. Bulk Force Parameters

The bulk parameters of interest for the Eros force environment are its total mass, volume, density, moments of inertia, and rotational velocity vector. Listed in Table 1 are the estimated values of these parameters [8].

A few items of interest related to the measured models should be noted. First is that the internal mass-density distribution of Eros seems remarkably homogeneous. The main observed deviations from this homogeneity lie at the resolution limit of the gravity field determination, and are statistically significant but of small magnitude, as can be seen in Fig. 1. Despite this, there is some evidence for a regolith covering on the surface of the asteroid with a different bulk density [3,8].

Second is the apparently uniform rotation of the asteroid. Specifically, no free precession of the asteroid has been directly measured from the navigation data. Estimates on the forced and free precession indicate that the polar motion should have a maximum amplitude of 0.02 deg over 6 months. The small amplitude of these motions indicates that Eros is essentially in uniform rotation about its maximum moment of inertia.

Table 1. Nominal parameters for Eros.

Parameter	Value	Unit
μ	$(4.4631 \pm 0.0003) \times 10^{-4}$	km^3/s^2
Volume	2503 ± 25	km^3
Density	2.67 ± 0.03	g/cm^3
Ixx (normalized)	17.09	km^2
Iyy (normalized)	71.79	km^2
Izz (normalized)	74.49	km^2
Pole right ascension	11.369 ± 0.003	deg
Pole declination	17.227 ± 0.006	deg
Rotation rate	1639.38885 ± 0.0005	deg/day

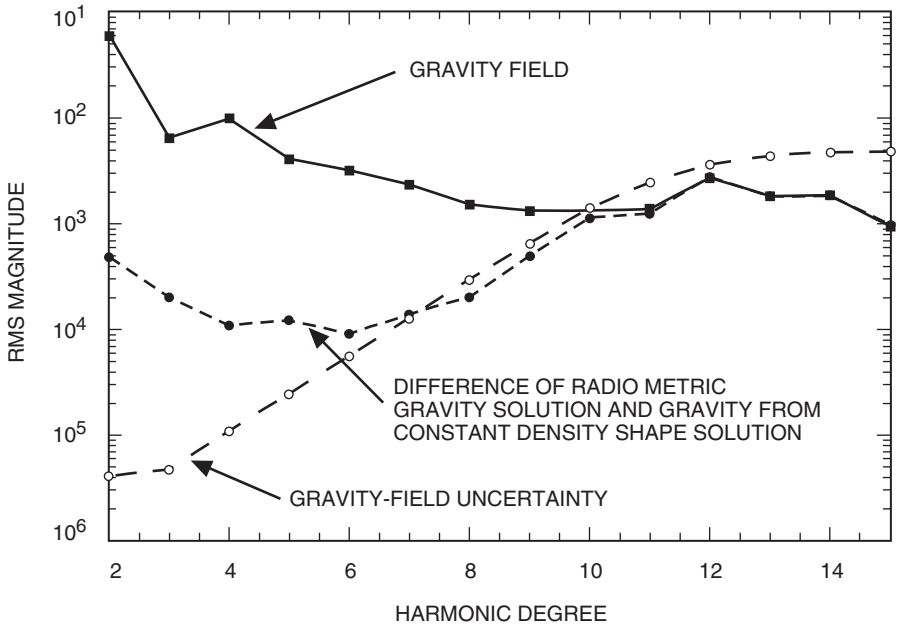

Fig. 1. Accuracy of gravity-field determination.

B. Gravity Field

Two basic models were used to represent the NEAR gravity field. The most accurate model is the spherical harmonic expansion of the field, as the coefficients of this expansion were directly determined from the spacecraft tracking data. However, this expansion diverges within the circumscribing sphere about Eros, negating its use for near-surface operations. In this regime, the NEAR mission used the constant density polyhedron model [16] for computing the gravity field. This computation is less accurate as it relies on the measured shape model plus the determined bulk density, and does not account for the small, but statistically significant, density inhomogeneities present in the asteroid.

The spherical harmonic gravity potential is specified as [4]

$$U = \frac{\mu}{r} \sum_{n=0}^{\infty} \sum_{m=0}^{n} \left(\frac{r}{r_o} \right)^n \bar{P}_{nm}(\sin\phi) \left[\bar{C}_{nm} \cos(m\lambda) + \bar{S}_{nm} \sin(m\lambda) \right] \tag{1}$$

or can be expressed in a perturbation form as

$$U = \frac{\mu}{|\mathbf{r}|} + R(\mathbf{r}) \tag{2}$$

where n is the degree and m is the order, $\bar{C}_{nm}$ and $\bar{S}_{nm}$ are the normalized gravity coefficients (listed in Table 2 up to degree and order 4), $\bar{P}_{nm}$ are the fully normalized Legendre polynomials and associated functions, r_o is the reference radius of Eros (assumed to be 16.0 km for the NEAR mission), ϕ is the latitude, and λ is the longitude. The normalized coefficients are related to the unnormalized ones by the relation

$$\left(\bar{C}_{nm}; \bar{S}_{nm} \right) = \sqrt{\frac{(n+m)!}{(2-\delta_{0m})(2n+1)(n-m)!}} \left(C_{nm}; S_{nm} \right) \tag{3}$$

Table 2. Normalized gravity coefficients, measured from the spacecraft dynamics and computed from the measured shape with a constant density assumption.

Coefficient ($r_0 = 16.0$ km)	Solution spacecraft dynamics	Solution shape-model integration
C_{10}	0	0.001175
C_{11}	0	−0.000348
S_{11}	0	0.000088
C_{20}	−0.052478 (.000051)	−0.052851
C_{21}	0	0.000102
S_{21}	0	0.000012
C_{22}	0.082483 (.000061)	0.083148
S_{22}	−0.027909 (.000035)	−0.028197
C_{30}	−0.001400 (.000030)	−0.001747
C_{31}	0.004059 (.000006)	0.004086
S_{31}	0.003375 (.000006)	0.003401
C_{32}	0.001791 (.000016)	0.002127
S_{32}	−0.000691 (.000016)	−0.000840
C_{33}	−0.010373 (.000027)	−0.010492
S_{33}	−0.012104 (.000027)	−0.012216
C_{40}	0.012900 (.000070)	0.013077
C_{41}	−0.000106 (.000014)	−0.000145
S_{41}	0.000136 (.000015)	0.000165
C_{42}	−0.017488 (.000035)	−0.017647
S_{42}	0.004577 (.000030)	0.004624
C_{43}	−0.000320 (.000044)	−0.000313
S_{43}	−0.000141 (.000044)	−0.000194
C_{44}	0.017552 (.000062)	0.017694
S_{44}	−0.009009 (.000061)	−0.009118

C. Solar Effects

When the spacecraft is far from the asteroid, it must contend with strong perturbations from the solar gravity and radiation pressure. For precision navigation, detailed models of the solar radiation pressure model for the spacecraft were derived and used during the operations phase.[3] This level of detail is not necessary for understanding the basic effect of the solar radiation pressure on the spacecraft and how it impinges on the stability of motion. Thus, we will use a simple flat-plate model for the solar radiation pressure. To compute the solar effects, it is necessary to specify the Eros orbit relative to the Sun. The current best estimate of the orbit is shown in Table 3.[4]

[3] J. K. Miller and C. Helfrich, "NEAR Solar Pressure Parameters," JPL Interoffice Memorandum 312.B-95-682 (internal document), Jet Propulsion Laboratory, Pasadena, California, October 26, 1995.

[4] A. Konopliv, personal communication, Jet Propulsion Laboratory, Pasadena, California, September 26, 2000.

Table 3. Estimates of Eros heliocentric orbit.

Element	Epoch February 14, 2000, 16:00:00.0000 ET	
	Value	Unit
Cartesian		
X	$-1.372619235 \times 10^{8} \pm 9.46386 \times 10^{-3}$	km
Y	$-1.404571499 \times 10^{8} \pm 3.53961 \times 10^{-2}$	km
Z	$-1.045890113 \times 10^{8} \pm 5.66481 \times 10^{-2}$	km
$\dot{X}$	$+1.488152028 \times 10^{1} \pm 2.51308 \times 10^{-10}$	km/s
$\dot{Y}$	$-1.759628159 \times 10^{1} \pm 1.85131 \times 10^{-9}$	km/s
$\dot{Z}$	$-7.314516907 \times 10^{0} \pm 2.87203 \times 10^{-9}$	km/s
Orbital		
a	$2.181658374 \times 10^{8}$	km
e	0.222764914	—
i	30.805595	deg
ω	138.798959	deg
Ω	342.384153	deg
ν	107.814684	deg

For our ideal spacecraft model, the solar gravity and radiation pressure forces can be derived from a force potential written as

$$V_S = \frac{\mu_S - \beta}{|\mathbf{D}|} \tag{4}$$

where μ_S is the gravitation parameter of the Sun, $\mathbf{D}$ is the spacecraft position vector from the Sun, and β is the force parameter of the solar radiation pressure, computed from

$$\beta = \frac{G_1}{B} \tag{5}$$

where $G_1 \sim 1 \times 10^{8}$ kg km^3/s^2/m^2 and B is the spacecraft mass-to-area ratio (kg/m^2). For a spacecraft, this usually is computed by dividing the total spacecraft mass by the projected surface area of the solar arrays plus the projected area of the spacecraft bus. When computing B for a body with complex geometry, possible attitude dynamics, and specular and diffuse components of reflection, a conservative assumption is to take the maximum possible value for this parameter. For NEAR, the total surface area from the front of the spacecraft[5] is ∼11.25 m^2, and estimates of the NEAR spacecraft mass at rendezvous were ∼500 kg. This leads to a parameter $B \sim 44$ kg/m^2.

III. General Orbit Dynamics Description

The measured force parameters and models define the dynamical problem of motion in the vicinity of Eros. Depending on the values of the asteroid mass, heliocentric orbit, rotation state, and spacecraft mass-to-area ratio, the character of motion in these equations will take on a variety of forms. Specifically,

[5] J. K. Miller and C. Helfrich, op cit.

for smaller asteroids the regions where solar and gravity field perturbations are important can coincide, leading to very complicated dynamics. Eros, however, is large enough so that these regions of influence do not coincide, making it possible to distinguish between a far-field and a close-field regime.

The spacecraft equations of motion, with the solar gravity, solar radiation pressure, and asteroid gravity accounted for, can be stated in a Sun-centered, inertially oriented frame as

$$\ddot{\mathbf{D}} = \frac{\partial V_D}{\partial \mathbf{D}} \tag{6}$$

$$V_D = \frac{\mu_S - \beta}{|\mathbf{D}|} + \frac{\mu}{|\mathbf{D} - \mathbf{d}|} + R(\mathbf{D} - \mathbf{d}) + \frac{\mu}{d^2}\hat{\mathbf{d}} \cdot \mathbf{D} \tag{7}$$

where μ is the asteroid's gravitational parameter, $\mathbf{D}$ is the spacecraft position vector relative to the Sun, $\mathbf{d}$ is the asteroid position vector relative to the Sun, and $\dot{(-)}$ denotes differentiation with respect to time. The asteroid motion satisfies $\ddot{\mathbf{d}} = -\mu_S/d^3\mathbf{d}$.

To change to an asteroid-centered frame, we apply the transformation

$$\mathbf{D} = \mathbf{d} + \mathbf{R}_I \tag{8}$$

where $\mathbf{R}_I$ is the asteroid-centered vector, assumed to be in an inertial frame. Substituting these into Eq. (6) yields

$$\ddot{\mathbf{R}}_I = \frac{\partial V_D}{\partial \mathbf{R}_I} + \frac{\mu_S}{d^2}\hat{\mathbf{d}} \tag{9}$$

$$= \frac{\partial V_R}{\partial \mathbf{R}_I} \tag{10}$$

where $\hat{\mathbf{d}}$ is the unit vector pointing from the Sun to the asteroid and the new force potential is

$$V_R = \frac{\mu}{|\mathbf{R}_I|} + R(\mathbf{R}_I) + \frac{\mu_S - \beta}{|\mathbf{d} + \mathbf{R}_I|} + \frac{\mu_S + \mu}{d^2}\left(\hat{\mathbf{d}} \cdot \mathbf{R}_I\right) \tag{11}$$

The spacecraft always will be relatively close to the asteroid, meaning that $d \gg R_I$, and suggesting that the quantity $1/|\mathbf{d} + \mathbf{R}_I|$ be expanded, yielding

$$\frac{1}{|\mathbf{d} + \mathbf{r}|} = \frac{1}{d}\left[1 - \frac{1}{d}\hat{\mathbf{d}} \cdot \mathbf{r} - \frac{1}{2d^2}\left\{\mathbf{r} \cdot \mathbf{r} - 3\left(\hat{\mathbf{d}} \cdot \mathbf{r}\right)^2\right\}\right] + \cdots \tag{12}$$

Substituting for this expansion, and noting that $\mu_S \gg \beta \gg \mu$, we find the simplified form of the potential:

$$V(\mathbf{r}) = \frac{\mu}{|\mathbf{r}|} + R(\mathbf{r}) + \frac{\beta}{d^2}\hat{\mathbf{d}} \cdot \mathbf{r} - \frac{1}{2}\frac{\mu_S}{d^3}\left[\mathbf{r} \cdot \mathbf{r} - 3\left(\hat{\mathbf{d}} \cdot \mathbf{r}\right)^2\right] \tag{13}$$

yielding the final equations of motion:

$$\ddot{\mathbf{R}}_I = \frac{\partial V(\mathbf{R}_I)}{\partial \mathbf{R}_I} \tag{14}$$

In the course of analyzing motion about an asteroid, it often is convenient to use the constants of motion of the two-body problem in order to characterize the strength and effect of the perturbations acting on the spacecraft. We will introduce these ideas throughout the article and, thus, will introduce the necessary notation here.

The classical orbital elements usually defined for a spacecraft can be given as the semi-major axis, a; the eccentricity, e; the inclination, i; the longitude of the ascending node, Ω; and the argument of periapsis, ω. Frequently, we will use the true anomaly of the orbit, f, to replace the classical sixth orbit element of the time of periapsis passage. The variation of these constants due to orbital perturbations generally is specified using the Lagrange planetary equations with a perturbation function. An extended discussion of these equations can be found in [2]. For our system, the general force perturbation potential can be given as

$$\mathcal{R}(\mathbf{r}) = R(\mathbf{r}) + \frac{\beta}{d^2}\hat{\mathbf{d}} \cdot \mathbf{r} - \frac{1}{2}\frac{\mu_S}{d^3}\left[\mathbf{r} \cdot \mathbf{r} - 3\left(\hat{\mathbf{d}} \cdot \mathbf{r}\right)^2\right] \tag{15}$$

and combines both gravity field and solar perturbations.

For some specific discussions, it is convenient to refer to a more basic set of two-body-problem constants of motion, the energy and angular momentum. For our applications, we will refer on occasion to the two-body energy, or Keplerian energy, C; the angular momentum magnitude, G; and the projection of the angular momentum onto the axis of rotation of the coordinate system, H. These are defined as

$$C = -\frac{\mu}{2a} \tag{16}$$

$$G = \sqrt{\mu a(1-e^2)} \tag{17}$$

$$H = G\cos i \tag{18}$$

The Lagrange equations for these elements are particularly simple and are listed later in the article.

IV. Dynamics in the Far-Field Regime

When relatively far from the asteroid, we can neglect the gravity-field perturbation terms and set the function $R = 0$ in the general equations of motion. Then the most important factor driving the forces acting on the spacecraft is the orbit of Eros about the Sun. The relatively high orbital eccentricity of Eros will cause variations in all of the perturbation terms. The essential parameters for this case are the Eros–Sun distance, d, and the true anomaly rate of Eros about the Sun, N:

$$d = \frac{p_S}{1 + e_S \cos\nu} \tag{19}$$

$$N = \frac{\sqrt{\mu_S p_S}}{d^2} \tag{20}$$

$$\dot{N} = -2\sqrt{\frac{\mu_S}{p_S}}\frac{e_S \sin\nu N}{d} \tag{21}$$

where μ_S is the Sun gravitational parameter, p_S is the Eros orbit parameter, e_S is the Eros orbit eccentricity, ν is the Eros true anomaly about the Sun, and $N = \dot{\nu}$ is the rate of change of the true anomaly. The angular velocity vector of the orbit about the Sun, $\mathbf{N}$, has a constant direction with a varying magnitude changing in accord with the above relations.

A. Equations of Motion

Now transform Eq. (14) into a frame that rotates with the asteroid about the Sun, which fixes the vector $\hat{\mathbf{d}}$. Introduce the vector $\mathbf{R}$ as the spacecraft position in this rotating frame to find the new equations of motion:

$$\ddot{\mathbf{R}} + 2\mathbf{N} \times \dot{\mathbf{R}} + \mathbf{N} \times \mathbf{N} \times \mathbf{R} + \dot{\mathbf{N}} \times \mathbf{R} = \frac{\partial V(\mathbf{R})}{\partial \mathbf{R}} \tag{22}$$

The left-hand side of the equations of motion corresponds to the acceleration of a vector in an arbitrarily rotating frame and is periodic with period equal to the asteroid orbital period about the Sun.

Now we introduce the so-called "pulsating frame," where the spacecraft position is scaled by the asteroid–Sun distance, d, and time is replaced with the asteroid true anomaly, ν. Although somewhat complicated, the introduction of this frame is essential in deriving equations of motion that can be stated in a simple form and analyzed in this regime. For our case, we scale the position vector by both the asteroid–Sun distance and by the small parameter $\epsilon = (\mu/\mu_S)^{1/3}$, as in the standard derivation of Hill's equations. The relationships between the vector $\mathbf{R}$ and its time derivatives and the new vector $\mathbf{r}$ and its asteroid true anomaly derivatives are

$$\mathbf{R} = \epsilon d \mathbf{r} \tag{23}$$

$$\dot{\mathbf{R}} = \epsilon N \left(d' \mathbf{r} + d \mathbf{r}' \right) \tag{24}$$

$$\ddot{\mathbf{R}} = \epsilon N \left(N' d' + N d'' \right) \mathbf{r} + \epsilon N \left(N' d + 2 N d' \right) \mathbf{r}' + \epsilon N^2 d \mathbf{r}'' \tag{25}$$

where $\mathbf{r}$ is the new position vector in this frame and $\mathbf{r}'$ denotes the derivative of this vector with respect to the asteroid true anomaly.

Substituting these relationships into Eq. (22), simplifying, and dividing through by the factor $\epsilon N^2 d$ results in the vector equation:

$$\mathbf{r}'' + 2\hat{\mathbf{z}} \times \mathbf{r}' + (\hat{\mathbf{z}} \cdot \mathbf{r}) \hat{\mathbf{z}} = \frac{1}{1 + e_S \cos \nu} \frac{\partial U}{\partial \mathbf{r}} \tag{26}$$

$$U = \frac{1}{|\mathbf{r}|} + \tilde{\beta} \hat{\mathbf{d}} \cdot \mathbf{r} + \frac{3}{2} \left(\hat{\mathbf{d}} \cdot \mathbf{r} \right)^2 \tag{27}$$

where $\tilde{\beta} = \beta / (\mu_S \epsilon)$. It is significant to note that Eq. (26) contains only two parameters, the eccentricity of the asteroid orbit, e_S, and the normalized effect of the solar radiation pressure (SRP) force, $\tilde{\beta}$, and that the equations are time periodic in the asteroid true anomaly, ν. These equations have a close affinity with the classical equations for the elliptic restricted three-body problem, with the addition that Hill's approximation has been applied and that they include the effect of the solar radiation pressure. Rewriting the equations in scalar form (assuming that $\hat{\mathbf{d}} = \hat{\mathbf{x}}$) yields

$$x'' - 2y' = \frac{1}{1 + e_S \cos\nu}\left[-\frac{x}{r^3} + \tilde{\beta} + 3x\right] \tag{28}$$

$$y'' + 2x' = \frac{1}{1 + e_S \cos\nu}\left[-\frac{y}{r^3}\right] \tag{29}$$

$$z'' + z = \frac{1}{1 + e_S \cos\nu}\left[-\frac{z}{r^3}\right] \tag{30}$$

The parameter $\tilde{\beta}$ is constant and describes the relative acceleration of the SRP on the spacecraft. For the NEAR spacecraft at Eros, $\tilde{\beta} \sim 1.14$. For comparison, the Rosetta spacecraft at comet Wirtanen and the Muses-C spacecraft at asteroid 25143 (1998 SF36) will have values of $\tilde{\beta} \sim 30$, while planetary orbiters will have $\tilde{\beta} \ll 1$.

B. An Algebraic Relation

These equations have an algebraic relation related to the Jacobi integral. Multiplying Eqs. (28) through (30) by x', y', and z', respectively, summing them up, treating the term $(1 + e_S \cos\nu)$ as a constant, and integrating yields

$$C = \frac{1}{2}\left(v^2 + z^2\right) - \frac{U(\mathbf{r})}{1 + e_S \cos\nu} \tag{31}$$

$$U(\mathbf{r}) = \frac{1}{r} + \tilde{\beta}x + \frac{3}{2}x^2 \tag{32}$$

where $v^2 = x'^2 + y'^2 + z'^2$. This expression is only a constant of integration in the special case when the asteroid is in a circular orbit about the Sun ($e_S = 0$). It serves a useful purpose, however, in establishing a sufficient criterion for spacecraft capture at the asteroid. The condition itself is a function of true anomaly, and a previously captured spacecraft can subsequently escape, but before escape can occur the criterion must first become violated. Following Marchal [6], we re-express Eq. (31) as

$$\Gamma = 2U(\mathbf{r}) - (1 + e_S \cos\nu)\left[v^2 + z^2\right] \tag{33}$$

The complete differential of Γ with respect to true anomaly yields

$$\Gamma' = e_S \sin\nu\left[v^2 + z^2\right] \tag{34}$$

showing that this quantity is only conserved for a circular orbit about the Sun.

C. Stability of Far-Field Motion against Escape

Using Eq. (33), it is possible to construct a necessary condition for the escape of a spacecraft from the asteroid, due to tidal and radiation pressure effects. To derive this result, consider the planar ($z = 0$) zero-velocity curves, as then the relationship becomes invariant with respect to asteroid true anomaly:

$$\Gamma = 2U(x, y, z = 0) \tag{35}$$

Thus, even though Γ itself is not constant, we can still derive boundaries for bounded motion that are constant—analogous to the circular Hill problem. Shown in Fig. 2 are zero-velocity curves for Eq. (35). It

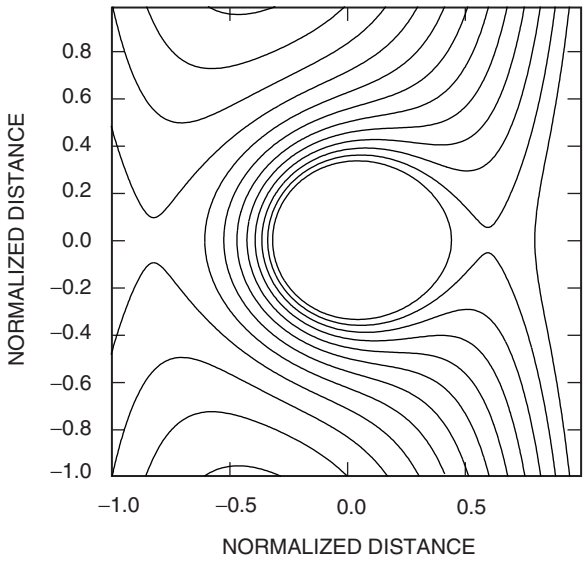

Fig. 2. Generic zero-velocity curve for $\tilde{\beta} > 1$.

is significant to note that the equilibrium points serve the same function in these curves as in the standard circular problem, as they denote the points at which the region containing the asteroid connect the regions that are separated from the asteroid. The value of Γ at the equilibrium points (also a constant) then becomes a useful criterion for whether the spacecraft is guaranteed to be bound to the asteroid or not, valid independent of asteroid true anomaly.

The equilibrium points for this problem correspond to co-orbital motion about the asteroid, accounting for solar radiation pressure and asteroid attraction. These are just equilibrium solutions to Eqs. (28) through (30), and for large and small values of $\tilde{\beta}$ are computed as $y^* = z^* = 0$ and

$$x^* \sim \pm\left(\frac{1}{3}\right)^{1/3} - \frac{\tilde{\beta}}{9} \pm \frac{3^{1/3}}{81}\tilde{\beta}^2 + \cdots \tag{36}$$

for $\tilde{\beta} \ll 1$ and are computed as

$$x^* \sim \begin{cases} -\dfrac{1}{3}\tilde{\beta} - \dfrac{9}{\tilde{\beta}^2} + \cdots & x^* < 0 \\ \dfrac{1}{\sqrt{\tilde{\beta}}} - \dfrac{3}{2\tilde{\beta}^2} + \cdots & x^* > 0 \end{cases} \tag{37}$$

for $\tilde{\beta} \gg 1$. Figure 3 shows comparisons of the leading order of these expansions to numerical solutions of the equilibrium solutions.

For $\tilde{\beta} \ll 1$, the value of Γ at the equilibrium points is

$$\Gamma^*_{\pm} \sim 3^{4/3} \pm 2\left(\frac{1}{3}\right)^{1/3}\tilde{\beta} - \frac{2}{9}\tilde{\beta}^2 + \cdots \tag{38}$$

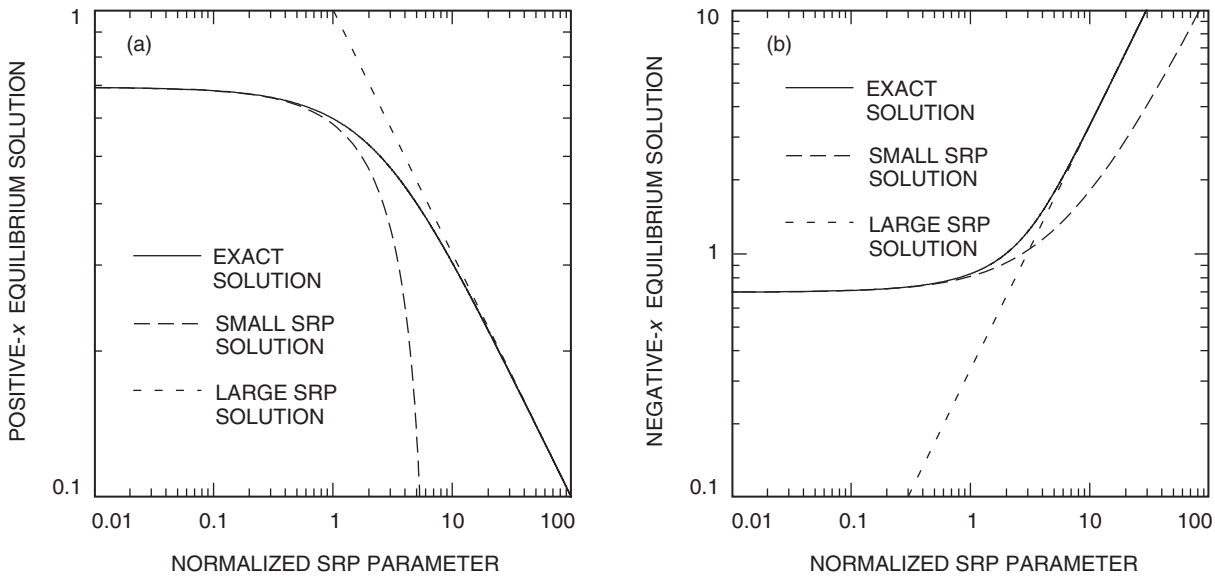

Fig. 3. Equilibrium points: (a) positive *x* and (b) negative *x*.

while for $\tilde{\beta} \gg 1$ the value is computed to be

$$\Gamma_+^* \sim 4\sqrt{\tilde{\beta}} + \cdots \tag{39}$$

for $x^* > 0$ and

$$\Gamma_-^* \sim -\frac{1}{3}\tilde{\beta}^2 + \cdots \tag{40}$$

for $x^* < 0$. From the values given above, it is clear that for $\Gamma > \Gamma_+^*$ the region surrounding the body is separated from the rest of space.

Combining the previous results, we see that there is a simple sufficient criterion for the capture of a spacecraft at a asteroid. When the current value of Γ for a spacecraft is greater than Γ_+^*, and the spacecraft is inside of the zero-velocity surface, then the spacecraft is definitely bound to the asteroid. Since the value of Γ changes over time, meeting the criterion at one time does not guarantee that it will be satisfied at some point in the future, so its use is somewhat limited. This does fit well, however, with using the criterion for a spacecraft mission as operations generally will focus on shorter time spans over which this criterion provides useful results.

To apply this sufficient condition to the stability of an orbit about an asteroid, the value of Γ should be computed along with the trajectory of the spacecraft. If the trajectory has sustained periods where the condition $\Gamma > \Gamma_+^*$ is violated, then this trajectory is a candidate for ejection from the asteroid. On the other hand, should the condition be satisfied throughout the time period of interest, the trajectory is guaranteed to be bound to the asteroid.

If the nominal spacecraft orbit is relatively close to the asteroid, then the semi-major axis will become relatively small as compared with the orbit energy. Using this as a justification, in Scheeres and Marzari [11] the approximate result is found:

$$\Gamma \sim \frac{\epsilon d}{a} \tag{41}$$

It is important to note that Γ is multiplied by the asteroid–Sun distance, meaning that even if a spacecraft were in an orbit with constant orbital elements, the value of Γ would decrease as the asteroid neared the Sun and increase as the asteroid moved away from the Sun. This is the mechanism that can cause a previously stable trajectory about a asteroid to become unstable near perihelion—allowing the spacecraft to be ejected from its orbit about the asteroid.

Using this to evaluate the stability condition for both small and large values of $\tilde{\beta}$ yields

$$a < \begin{cases} \dfrac{1}{3^{4/3}} \left(\dfrac{\mu}{\mu_S}\right)^{1/3} d & \text{for } \tilde{\beta} \ll 1 \\ \left(\dfrac{\mu}{\mu_S}\right)^{1/3} \dfrac{d}{4\sqrt{\tilde{\beta}}} & \text{for } \tilde{\beta} \gg 1 \end{cases} \tag{42}$$

V. Dynamics in the Near-Field Regime

A. Equations of Motion

For the analysis of motion close to the asteroid, we shift our focus from motion relative to the asteroid–Sun line to motion relative to the rotating asteroid. To simplify the dynamical description of motion relative to the asteroid, we shift to the asteroid-fixed frame. Since the asteroid is uniformly rotating with an angular velocity vector $\mathbf{\Omega}$ with respect to inertial space, the equations of motion relative to the asteroid have the form

$$\ddot{\mathbf{r}} + 2\mathbf{\Omega} \times \dot{\mathbf{r}} + \mathbf{\Omega} \times \mathbf{\Omega} \times \mathbf{r} = \frac{\partial V(\mathbf{r})}{\partial \mathbf{r}} \tag{43}$$

where $\mathbf{r}$ denotes the position vector in the body-fixed space and V is computed from Eq. (13). In this frame, the vector $\hat{\mathbf{d}}$ controls the direction in which the solar perturbations act, and is the direction of the Sun relative to the asteroid surface. Resolving the equations into a specific body-fixed Cartesian frame yields

$$\ddot{x} - 2\omega_E \dot{y} = \omega_E^2 x - \frac{\mu}{r^3} x + \frac{\partial R}{\partial x} - \frac{\mu_S}{d^3} x + \left[\frac{\beta}{d^2} + \frac{\mu_S}{d^3}\left(\hat{\mathbf{d}} \cdot \mathbf{r}\right)\right] \hat{d}_x \tag{44}$$

$$\ddot{y} + 2\omega_E \dot{x} = \omega_E^2 y - \frac{\mu}{r^3} y + \frac{\partial R}{\partial y} - \frac{\mu_S}{d^3} y + \left[\frac{\beta}{d^2} + \frac{\mu_S}{d^3}\left(\hat{\mathbf{d}} \cdot \mathbf{r}\right)\right] \hat{d}_y \tag{45}$$

$$\ddot{z} = -\frac{\mu}{r^3} z + \frac{\partial R}{\partial z} - \frac{\mu_S}{d^3} z + \left[\frac{\beta}{d^2} + \frac{\mu_S}{d^3}\left(\hat{\mathbf{d}} \cdot \mathbf{r}\right)\right] \hat{d}_z \tag{46}$$

where x, y, and z are generally measured along the asteroid's minimum, intermediate, and maximum moment of inertia axes in the body-fixed frame and ω_E is the rotation rate of the asteroid. The terms

d and $\hat{\mathbf{d}}$ will vary in time as the asteroid moves about the Sun and as the asteroid rotates in inertial space.

In general, these equations of motion will have no integrals of their motion. However, for motion close to Eros, we can disregard terms of the order μ_S/d^3 and β/d^2 relative to the gravity field. Then the resulting equations are time invariant and the Jacobi integral exists:

$$J = \frac{1}{2}\left(\dot{x}^2 + \dot{y}^2 + \dot{z}^2\right) - \frac{1}{2}\omega_E^2\left(x^2 + y^2\right) - \frac{\mu}{r} - R \tag{47}$$

B. Stability of Near-Field Motion against Impact

The Jacobi integral in the near-field motion can be used to construct a barrier to impact with the asteroid surface. The zero-velocity curves of this system are found by computing the contours of the gravity-plus-centripetal potential in the body-fixed position space, x, y, and z, where J denotes a particular value of the Jacobi constant. These contour lines then define the limits of physical motion that a spacecraft can have in the body-fixed space, given that value of the Jacobi constant. In general, the spacecraft dynamics must satisfy the inequality constraint:

$$U + \frac{1}{2}\omega_E^2\left(x^2 + y^2\right) + J \geq 0 \tag{48}$$

which constrains the spacecraft to lie on one side of the zero-velocity curves. Figure 4 shows the zero-velocity curves corresponding to the Eros shape model.

For the purpose of characterizing spacecraft dynamics about this body, we are primarily interested in finding the value of the Jacobi constant such that, for all values of J less than this, the zero-velocity curves

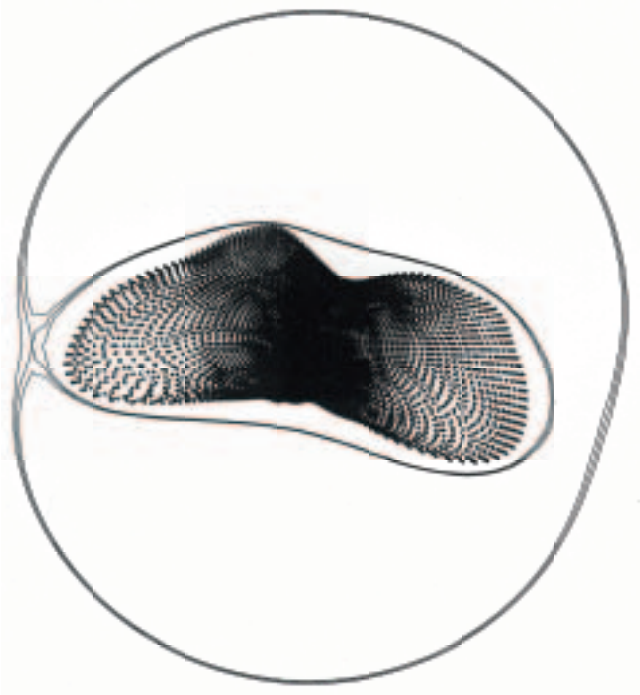

Fig. 4. Zero-velocity curve for motion close to Eros.

are guaranteed to separate the trajectory space containing the asteroid and the space not containing the asteroid. Then we have explicitly that a spacecraft in orbit in the outer region with the appropriate Jacobi integral value can never, under gravitational dynamics alone, impact onto the asteroid surface. For the Eros gravity field, $J_o = -4.9 \times 10^{-5}$ km^2/s^2 and corresponds to the equilibrium point shown in the zero-velocity curve. To ensure stability against impact, we must choose the initial spacecraft conditions such that the spacecraft position resides in the outer portion of the zero-velocity curve and that the value of the Jacobi integral is less than or equal to J_o:

$$C - \omega_E H - R \leq J_o \tag{49}$$

which provides a simple check in terms of osculating orbital elements for whether or not the spacecraft might impact with the surface at some point in the future. This relation can be expressed in terms of initial osculating elements for an assumed direct, equatorial orbit specified by its periapsis radius, eccentricity, and initial longitude λ in the body-fixed frame:

$$\frac{-\mu(1-e)}{2r_p} + \omega_E \sqrt{\mu r_p (1+e)} + R(r = r_p, \lambda) + J_o = 0 \tag{50}$$

Figure 5 shows a plot of the limiting stability against impact curve for the Eros system (including the full effect of the gravity field) in terms of initial periapsis radius and eccentricity for an equatorial orbit. To find this curve, the family of curves for values of $\lambda \in [0, 360]$ deg were generated and the limiting curve to the right (into the impact stability region) was found. Note that this curve is significantly shifted as compared with the results given earlier, which were based on the initial NEAR flyby of the asteroid [12].

While this result is sharp, it is limited to the orbits that have relatively low inclination. For orbits with higher inclinations, this result becomes less useful and doesn't place any real limits on spacecraft motion. In these regions, different approaches to the problem are needed.

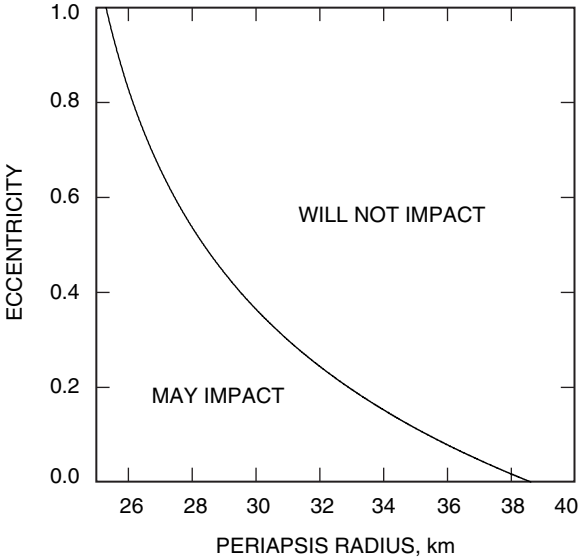

Fig. 5. Stability against impact curve for equatorial, direct orbits. Initial orbits to the left of this line may impact with Eros at some point in the future; orbits to the right of this line will not impact with Eros.

C. Stability Limits in Phase Space

In addition to the Hill-stability results found above, it also is possible to characterize the local stability of orbital motion. In this approach, one considers a certain orbit and computes the linear characteristics of motion to determine if neighboring trajectories will remain close to the trajectory or will diverge from it. Such analysis generally is applied to periodic orbits and is described in greater detail in [12]. For Eros, we have applied this approach to families of near-equatorial direct and retrograde orbits in order to characterize the minimum orbital radius for linearly stable motion. When relatively far from the asteroid, orbits will be stable as the perturbations from the gravity field diminish with distance. Conversely, when close to the asteroid, the motion will be unstable, indicating that the gravity field perturbations have become large enough to seriously disrupt the motion. In this approach, we compute the distance at which near-circular orbits transition from stable to unstable, providing an indication of the stability limit.

The transition from stable to unstable circular orbits in the equatorial plane (inclination $\sim$0) occurs at a radius of 33.4 km, a slight shift from the results reported previously [12]. This particular limit is only of theoretical interest as an orbiter perturbed sufficiently from these "stable" circular orbits will feel strong perturbations from the rotating Eros gravity field. It also is important to note that this is within the Hill stability limit for impact on the surface, showing that the limiting members of these periodic orbits theoretically can transition into impacting trajectories if given a sufficient perturbation. Backing off a few kilometers to orbits outside of 34 km will ensure stability against impact, although the orbit still may experience an escape.

The transition from stable to unstable circular orbits retrograde in the equatorial plane (inclination $\sim$180 deg) now occurs at a radius of 20.8 km (again close to the previously reported value [12]). This particular limit is of practical interest since the NEAR mission plan included an extended period of low-radius, retrograde, near-equatorial, near-circular orbits. This stability transition corresponds to an intersection of the retrograde circular orbits with an out-of-plane family of twice the period.

Currently, work is being done to characterize the stability of motion using three-dimensional periodic orbit families. In [5], the stability transitions for three-dimensional periodic orbits about Eros were investigated. The periodic orbits used to compute the stability transitions bifurcate from planar orbits with resonance between the asteroid rotation rate and the out-of-plane frequency. Results of this analysis are shown in Fig. 6. This figure shows the transition from stable regions to unstable regions as inclination changes from retrograde to direct for different values of the semi-major axis.

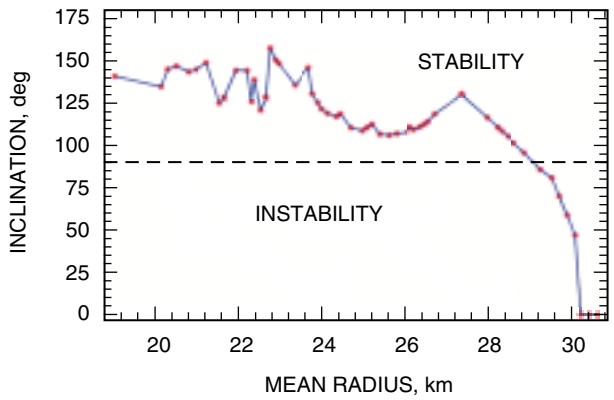

Fig. 6. Stability regions for three-dimensional motion around the asteroid Eros.

D. Analytical Stability Analysis of Polar Orbits

Polar orbits and the global coverage they provide were of particular interest to the NEAR mission and to any asteroid-mapping experiment. In fact, the NEAR mission had an extended period in a polar orbit, and there was interest in decreasing the orbit radius as much as possible to gain additional signal in the gravitational measurements. During the mission, it was determined numerically that polar orbits had a lower limit on radius that, if violated, soon led to unstable (escaping) orbital motion.

It is, in fact, possible to better understand this lower limit using classical analytical and averaging techniques combined with more modern characterizations found for asteroid orbiters. To better understand the dynamics in this particular case, we must consider the combined effects of the C_{20}, C_{30}, and C_{40} gravity coefficients on a polar orbit, represented by the potential contributions:

$$U_{20} = \frac{\mu r_o^2 C_{20}}{r^3}\left(1 - \frac{3}{2}\cos^2\delta\right) \tag{51}$$

$$U_{30} = \frac{\mu r_o^3 C_{30}}{2r^4}\sin\delta\left(5\sin^2\delta - 3\right) \tag{52}$$

$$U_{40} = \frac{\mu r_o^4 C_{40}}{8r^5}\left[35\sin^4\delta - 40\sin^2\delta + 3\right] \tag{53}$$

$$\sin\delta = \sin i \sin(\omega + f) \tag{54}$$

Each of these terms can be averaged over one spacecraft orbit, yielding the secular potentials:

$$\bar{U}_{20} = \frac{\mu r_o^2 C_{20}}{2a^3(1-e^2)^{3/2}}\left(\frac{3}{2}\sin^2 i - 1\right) \tag{55}$$

$$\bar{U}_{30} = \frac{3\mu r_o^3 C_{30}}{2a^4(1-e^2)^{5/2}}\sin i \sin\omega e\left(\frac{5}{4}\sin^2 i - 1\right) \tag{56}$$

$$\bar{U}_{40} = \frac{3\mu r_o^4 C_{40}}{8a^5(1-e^2)^{7/2}}\left[\left(\frac{35}{8}\sin^4 i - 5\sin^2 i + 1\right)\left(1 + \frac{3}{2}e^2\right) + \frac{5}{4}\sin^2 i\cos(2\omega)\left(3 - \frac{7}{2}\sin^2 i\right)e^2\right] \tag{57}$$

Of particular interest to us is the evolution of the eccentricity, which follows the basic equation:

$$\dot{e} = -\frac{\sqrt{1-e^2}}{na^2 e}\frac{\partial R}{\partial \omega} \tag{58}$$

$$e' = -\frac{r^2}{\mu a e}\frac{\partial R}{\partial \omega} \tag{59}$$

$$n = \sqrt{\frac{\mu}{a^3}} \tag{60}$$

where e' denotes differentiation with respect to orbit true anomaly. We also should note the familiar result from the standard averaging analysis of C_{20}, that the argument of periapsis has a secular component defined as

$$\dot{w} = \frac{3nr_o^2 C_{20}}{2a^2(1-e^2)^2}\left(\frac{5}{2}\sin^2 i - 2\right) \tag{61}$$

meaning that the argument of periapsis will have a constant rate of change on average, and that the eccentricity will have no secular evolution due to this gravity term.

What is observed numerically for orbiters near Eros, however, is a large transient oscillation in eccentricity that causes the orbit periapsis occasionally to dip closer or farther from the asteroid. As established previously in [12], it is the orbit periapsis and eccentricity that control the coupling of the asteroid gravity field to the orbit dynamics, and periapsis passages at a close enough distance can rapidly destabilize the motion. Thus, it is of interest to characterize analytically the expected variations in eccentricity due to the gravity field perturbations. To do this, we will look at the transient variations in eccentricity due to C_{20}, and at the long-period variations in eccentricity due to C_{30} and C_{40} combined with the secular motion of the argument of periapsis. In the following, we will make the assumption that the orbit is near-circular and, thus, that we can ignore higher orders of eccentricity.

First we note that the differential equation for eccentricity with respect to C_{20} can be written as

$$e' = \frac{3}{2}\frac{C_{20}\sin^2 i}{a^2}\left[\sin(2\omega)\big(\cos(3f)+\cos(f)\big) + \cos(2\omega)\big(\sin(3f)+\sin(f)\big) + \mathcal{O}(e)\right] \tag{62}$$

which can be integrated with respect to true anomaly to yield

$$\Delta e_{20} = \frac{3}{2}\frac{C_{20}\sin^2 i}{a^2}\left[\sin(2\omega)\left(\frac{1}{3}\sin(3f)+\sin(f)\right) + \cos(2\omega)\left(\frac{1}{3}\big(1-\cos(3f)\big)+1-\cos(f)\right) + \mathcal{O}(e)\right] \tag{63}$$

This gives the amplitude of the eccentricity fluctuation about its mean value, which must still be computed. This is found by taking the average of the above equation over one orbit, or

$$\bar{\Delta e}_{20} = \frac{1}{2\pi}\int_0^{2\pi} \Delta e dM \tag{64}$$

$$= \frac{2r_o^2 C_{20}}{a^2}\sin^2 i\cos(2\omega) + \mathcal{O}(e) \tag{65}$$

Thus, the total fluctuation in eccentricity due to C_{20} is computed as $\bar{\Delta e}_{20} + \Delta e_{20}$, for which a reasonable bound can be found:

$$\bar{\Delta e}_{20} + \Delta e_{20} \leq \frac{10}{3}\frac{r_o^2 C_{20}}{a^2}\sin^2 i \tag{66}$$

This upper limit does not agree, however, with numerical integration of an orbit in the full gravitational field.

To analyze the contribution of C_{30} to the variation of e, we note that the differential equation for this term is

$$\dot{e}_{30} = -\frac{3}{2}\frac{nr_o^3 C_{30}}{a^3(1-e^2)^2}\left(\frac{5}{4}\sin^2 i - 1\right)\sin i\cos\omega \tag{67}$$

Now, the presence of $\cos\omega$ in the equation is important, as we note that this term will have a secular change due to C_{20}. Thus, we change the independent variable to ω to find

$$\frac{de_{30}}{d\omega} = \frac{\dot{e}_{30}}{\dot{\omega}_{20}} \tag{68}$$

$$= -\frac{1}{2}\frac{r_o^3 C_{30}}{ar_o^2 C_{20}}\sin i\cos\omega \tag{69}$$

which can be integrated immediately to find

$$\Delta e_{30} = -\frac{1}{2}\frac{r_o^3 C_{30}}{ar_o^2 C_{20}}\sin i\sin\omega \tag{70}$$

By combining an analysis of the effect of C_{20} and C_{30} on a near-circular, polar orbit, we find the following relation for the maximum value of eccentricity over one circulation period of the argument of periapsis:

$$e_{max} \sim \frac{10}{3}\frac{r_o^2|C_{20}|}{a^2} + \frac{r_o^3|C_{30}|}{ar_o^2|C_{20}|} \tag{71}$$

From this relation, we find that the maximum excursion in eccentricity is 0.125 for a 35-km orbit, 0.1 for a 40-km orbit, and 0.07 for a 50-km orbit. The equation is plotted in Fig. 7(a) for the values of Eros. The period of the oscillation is computed from secular C_{20} theory for the circulation in argument of periapsis:

$$T_\omega = \frac{8\pi}{3}\frac{a^{3.5}}{\sqrt{\mu}r_o^2|C_{20}|} \tag{72}$$

and is equal to 41 days in a 35-km orbit, 62 days in a 40-km orbit, and 142 days in a 50-km orbit. This long period oscillation in eccentricity does not seem to affect the long-term stability of the orbit until the semi-major axis drops below 35 km. These approximate limits and numerical integrations for long-term stable orbits seem to agree well [see Figs. 7(b) and 7(c)].

When the polar orbit radius drops below 35 km, it enters a region of stronger interaction with the rotating gravity field (see Figs. 3 and 4 in [12]). This also coincides with a 5:2 resonance at a =35 km and a 3:1 resonance at a =33 km between the orbit period and the rotating asteroid. The mechanism of the instability at this limit follows a pattern that involves the long-term eccentricity oscillation plus the (small) effect of the C_{40} gravity coefficient term.

As shown in Scheeres et al. [12], the strength of the Eros–orbit interactions increases with eccentricity. Thus, an initially circular orbit at a semi-major axis of 33 km will experience a mounting perturbation as the eccentricity increases (due to C_{20} and C_{30}). However, numerical integration of the spacecraft motion

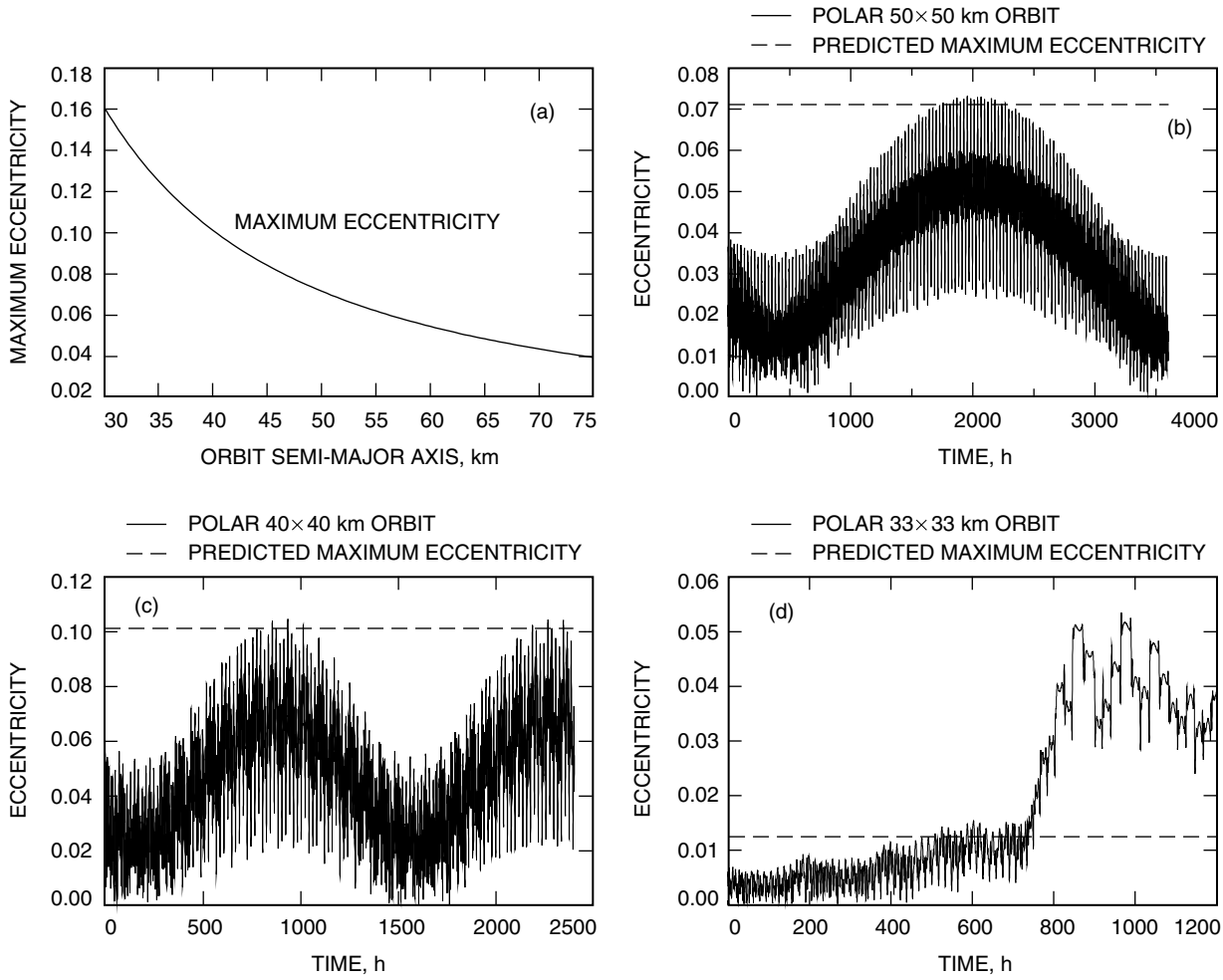

Fig. 7. Eccentricity: (a) maximum eccentricity due to C_{20} and C_{30} perturbations over one circulation period of the argument of periapsis, (b) eccentricity of a polar, 50 X 50 km orbit over one circulation period of argument of periapsis, (c) eccentricity of a polar, 40 X 40 km orbit over one circulation period of argument of periapsis, and (d) eccentricity of a polar, 33 X 33 km orbit over 50 days.

in an Eros gravity field taken to the third degree and order only, starting at this semi-major axis value, will not experience a long-term instability. This is due to the maximum eccentricity amplitude not being large enough to bring the orbit into a region of strong interaction with the gravity field. If we model the effect of the C_{40} gravity term, however, we see that it boosts the maximum eccentricity by a small amount, characterized as a function of argument of periapsis. To find this contribution, we consider the averaged equation for eccentricity due to this gravity term with respect to time and with respect to argument of periapsis:

$$\dot{e}_{40} = \frac{15}{16}\frac{nr_o^4 C_{40}}{a^4(1-e^2)^3}\left(3 - \frac{7}{2}\sin^2 i\right)\sin^2 i \sin(2\omega)e \tag{73}$$

$$\frac{de_{40}}{d\omega} = -\frac{15}{16}\frac{r_o^4 C_{40}}{a^2(1-e^2)r_o^2 C_{20}}\frac{\left(\frac{7}{6}\sin^2 i - 1\right)}{\left(\frac{5}{4}\sin^2 i - 1\right)}\sin(2\omega)e \tag{74}$$

Assuming small e again, and allowing the inclination to be equal to 90 deg gives us

$$e_{40} = e_o \exp\left[-\frac{5}{8}\frac{R_o^4 C_{40}}{a^2 R_o^2 C_{20}}\sin^2\omega\right] \tag{75}$$

At a semi-major axis of 35 km, we find that this perturbation can increase eccentricity by at most 4.5 percent. At $a = 33$ km, the effect of this gravity term is sufficient to nudge the orbit into a region of unstable motion, characterized by large changes in orbit energy and angular momentum from orbit to orbit. Numerical integrations back up this result, as is evident from Fig. 7(d).

For initial values of the semi-major axis chosen lower than ∼33 km, the long-term oscillation in eccentricity coupled with the increasing strength of the transient fluctuations in energy and angular momentum combine to make it infeasible to safely orbit the asteroid. It is interesting to note that this is approximately the same limit found for the linear stability of direct, near-equatorial orbits and agrees with the results in Fig. 6.

E. Effect of Transient Perturbations

In the extremely perturbed environment close to an asteroid such as Eros, the spacecraft can be subject to large changes in its orbital elements over a relatively short time period. Such situations have not arisen in classical astrodynamics, where perturbations are generally small and effects take many orbits or days to become significant. In the asteroid environment, however, large fluctuations in an orbit can be observed per orbit about the body, in many cases causing a chaotic evolution of an orbit leading to an impact or escape from the body. Even though these effects are large, it is possible to characterize them analytically and even to use them in the design of close-proximity operations [1,14].

For our analytical computations, it is more useful to use the "canonical" form of the Lagrange planetary equations [2], which expresses the change in orbit Keplerian energy, angular momentum, and angular momentum projected onto the z-axis as a function of the gravitational perturbations acting on them. The equations describing the change of these variables then can be expressed as

$$\frac{dC}{dt} = \frac{\partial R}{\partial t} \tag{76}$$

$$\frac{dG}{dt} = \frac{\partial R}{\partial \omega} \tag{77}$$

$$\frac{dH}{dt} = \frac{\partial R}{\partial \Omega} \tag{78}$$

where

$$C = \frac{-\mu}{2a} \tag{79}$$

$$G = \sqrt{\mu a(1-e^2)} \tag{80}$$

$$H = G\cos i \tag{81}$$

$$R = U - \frac{\mu}{r} \tag{82}$$

and a, e, i, ω, and Ω are the osculating orbital elements. Equations (77) and (78) are taken from classical results [2], while Eq. (76) is derived by applying the chain rule, taking the partial of R with respect to the true anomaly f first and then taking the partial of the true anomaly f with respect to the time [9]. Note that we neglect to add the additional equations describing the dynamics of the argument of periapsis, longitude of the ascending node, and mean epoch, as we will not explicitly study those equations here. The Jacobi integral can be restated in terms of these basic variables:

$$J = C - \omega_E H - R \tag{83}$$

The strongest perturbation that the trajectory feels when in close proximity to the asteroid is mainly due to the second-degree and -order gravity field of the rotating body [12], which has the explicit form

$$U_{20+22} = \frac{\mu R_o^2}{r^3}\left[C_{20}\left(1 - \frac{3}{2}\cos^2\delta\right) + 3C_{22}\cos^2\delta\cos 2\lambda\right] \tag{84}$$

For our analytical estimates, we will consider only the contribution from these terms.

Although the orbital dynamics are best computed using numerical integrations, a class of estimates for the change in orbit energy and angular momentum can be derived that provides a great deal of insight into the effect of a close flyby on the resulting orbit. The basic application of this theory is found in [10], and the results are restated here. Of particular interest is the change in orbit parameters as a spacecraft descends from a relatively high apoapsis to a periapsis close to the asteroid surface, and the change in orbit parameters as the spacecraft travels through a full orbit, from apoapsis to apoapsis. In the following, we state explicit formulae for the change in energy, C; angular momentum, G; and the projection of the angular momentum along the z axis, H. Changes in these parameters can be related to changes in the classical orbital elements [15].

1. Half-Orbit Perturbations. Over an orbit transfer from apoapsis to periapsis, we find variations in the orbital elements due to both the C_{20} and the C_{22} gravity coefficients.

The projected angular momentum, H, is identically conserved under perturbation from C_{20}, and thus will not vary. The energy and total angular momentum, C and G, will vary over a half orbit, however, yielding changes of

$$\Delta G_{C_{20}} = 2\sqrt{\frac{\mu}{p^3}}C_{20}\cos 2\omega \sin^2 ie \tag{85}$$

$$\Delta C_{C_{20}} = \frac{\mu}{2p^3}C_{20}\left[-1 + 3\left(\cos^2 i + \sin^2 i\cos 2\omega\right)\right]\left(3 + e^2\right)e \tag{86}$$

Similarly, and leading to more detailed results, the change in orbit elements C, G, and H due to C_{22} over one-half an orbit also can be predicted approximately:

$$\Delta G_{C_{22}} = -3C_{22}\sqrt{\frac{\mu}{p^3}}$$

$$\times \left[\cos^4\left(\frac{i}{2}\right)\left\{\sin 2(\omega+\Omega)I_2^1 + \cos 2(\omega+\Omega)J_2^1\right\}\right.$$

$$\left. + \sin^4\left(\frac{i}{2}\right)\left\{\sin 2(\omega-\Omega)I_{-2}^1 - \cos 2(\omega-\Omega)J_{-2}^1\right\}\right] \tag{87}$$

$$\Delta H_{C_{22}} = -3C_{22}\sqrt{\frac{\mu}{p^3}}\left[\frac{1}{2}\sin^2 i\left\{\sin 2\Omega I_0^1 + \cos 2\Omega J_0^1\right\}\right.$$

$$+ \cos^4\left(\frac{i}{2}\right)\left\{\sin 2(\omega+\Omega)I_2^1 + \cos 2(\omega+\Omega)J_2^1\right\}$$

$$\left. - \sin^4\left(\frac{i}{2}\right)\left\{\sin 2(\omega-\Omega)I_{-2}^1 - \cos 2(\omega-\Omega)J_{-2}^1\right\}\right] \tag{88}$$

and the variation in C can be found from the Jacobi integral. The integrals I_m^n and J_m^n have the definitions

$$I_m^n = 2\int_0^\pi (1+e\cos\nu)^n \cos(mf - 2\omega_E t)\, df \tag{89}$$

$$J_m^n = 2\int_0^\pi (1+e\cos\nu)^n \sin(mf - 2\omega_E t)\, df \tag{90}$$

These integrals cannot be expressed in closed form in general except for the particular cases:

$$I_0^{-2} = \frac{\sin\left(2\pi\sqrt{\omega_E^2 a^3/\mu}\right)}{\sqrt{\omega_E^2 p^3/\mu}} \tag{91}$$

$$J_0^{-2} = \frac{\cos\left(2\pi\sqrt{\omega_E^2 a^3/\mu}\right)}{\sqrt{\omega_E^2 p^3/\mu}} \tag{92}$$

The numerical quadrature of these integrals has been treated previously [10]. We note that these integrals are intimately related to the Hansen coefficients [13]. Figure 8 shows the values of these integrals over an interval of parameter values of interest. The total variation in these elements over an apoapsis-to-periapsis passage then is computed as

$$\Delta G = \Delta G_{C_{20}} + \Delta G_{C_{22}} \tag{93}$$

$$\Delta H = \Delta H_{C_{20}} + \Delta H_{C_{22}} \tag{94}$$

$$\Delta C = \Delta C_{C_{20}} + \Delta C_{C_{22}} \tag{95}$$

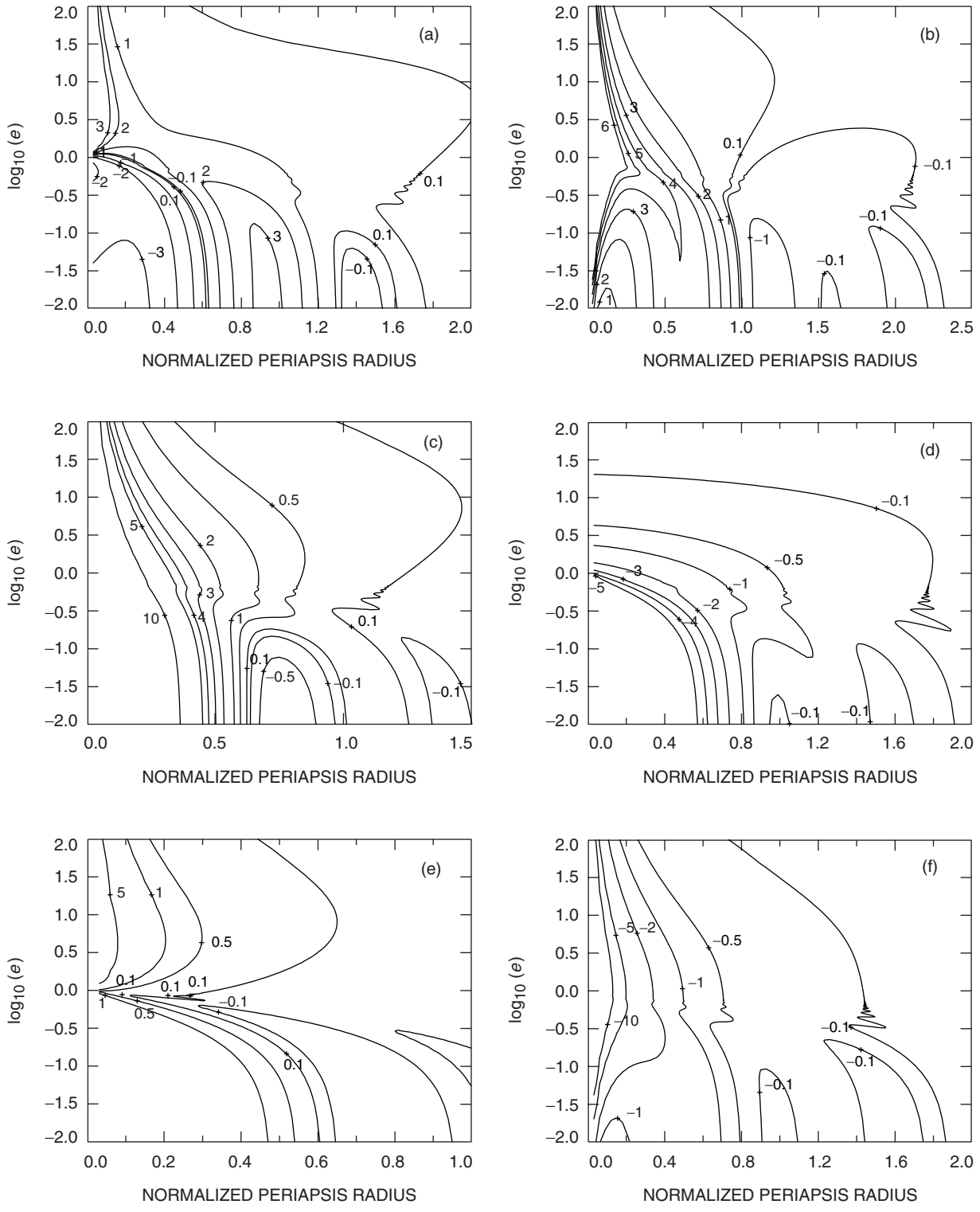

Fig. 8. Contour plots of integrals (a) $I_2^1/(2p^{3/2})$, (b) $J_2^1/(2p^{3/2})$, (c) $I_0^1/(2p^{3/2})$, (d) $J_0^1/(2p^{3/2})$, (e) $I_{-2}^1/(2p^{3/2})$, and (f) $J_{-2}^1/(2p^{3/2})$. The normalized periapsis radius is defined as $q(\omega^2/\mu)^{1/3}$, where q is the dimensional periapsis.

Using these results, it is possible to predict the change in orbital parameters between apoapsis of the transfer ellipse to periapsis of the ellipse. In general, the variation in energy and angular momentum can be quite large, implying that using Keplerian orbits to initiate numerical targeting routines may be an inefficient way in which to choose a target flyover condition. Rather, using the above relations in the initial design of a de-orbit maneuver can provide additional insight into the selection of target points on the asteroid surface.

2. Full-Orbit Perturbations. For analysis of the low-altitude flyovers, the orbit is continued through periapsis up to its next apoapsis passage, experiencing additional perturbations along the way. For the effect of the C_{20} gravity term, these additional perturbations erase the fluctuations in angular momentum and energy. For the C_{22} effects, however, only a partial cancellation occurs, leaving a residual change in the orbit elements that is often rather large [10,12]. The results are similar to the half-orbit results, except that the integrals J_m^n will cancel out over a full orbit pass, leaving only the terms containing the integrals I_m^n:

$$\begin{aligned}\Delta G = & -6C_{22}\sqrt{\frac{\mu}{p^3}} \\ & \times \left[\cos^4\left(\frac{i}{2}\right)\sin 2(\omega+\Omega)I_2^1 + \sin^4\left(\frac{i}{2}\right)\sin 2(\omega-\Omega)I_{-2}^1\right] \end{aligned} \tag{96}$$

$$\begin{aligned}\Delta H = & -6C_{22}\sqrt{\frac{\mu}{p^3}} \\ & \times \left[\frac{1}{2}\sin^2 i \sin 2\Omega I_0^1 + \cos^4\left(\frac{i}{2}\right)\sin 2(\omega+\Omega)I_2^1 - \sin^4\left(\frac{i}{2}\right)\sin 2(\omega-\Omega)I_{-2}^1\right] \end{aligned} \tag{97}$$

$$\begin{aligned}\Delta C = & -6C_{22}\omega_E\sqrt{\frac{\mu}{p^3}} \times \left[\frac{1}{2}\sin^2 i \sin 2\Omega \left\{I_0^1 - (1-e)^3 I_0^{-2}\right\}\right. \\ & + \cos^4\left(\frac{i}{2}\right)\sin 2(\omega+\Omega)\left\{I_2^1 - (1-e)^3 I_0^{-2}\right\} \\ & \left. - \sin^4\left(\frac{i}{2}\right)\sin 2(\omega-\Omega)\left\{I_{-2}^1 - (1-e)^3 I_0^{-2}\right\}\right] \end{aligned} \tag{98}$$

Note from Fig. 8 that $I_2^1 \gg I_{-2}^1$ and $I_2^1 \gg I_0^1$ in the regions of interest to us. Thus, direct, low-inclination orbits will be subject to the terms I_2^1 while retrograde, near-equatorial orbits primarily will be subject to the terms I_{-2}^1. Inspecting the contour plots, it is obvious that direct orbits will experience much larger changes in energy and angular momentum over each orbit, while the retrograde orbits will experience little, if any, change per orbit.

VI. Conclusions

In this article, we review the estimated force parameters for Eros as measured by the NEAR spacecraft. Then, using these parameter values as motivation, we discuss all significant elements of the orbital dynamics environment about Eros. The general equations of motion are derived, suitable for analytical and numerical study. These are then specialized to motion far from the asteroid and motion close to the

asteroid. Some specific analytical stability criteria are derived, as are some numerically based criteria. Finally, a qualitative approach to the description of orbital dynamics perturbations when close to the asteroid is presented and discussed.

References

[1] P. G. Antreasian, C. L. Helfrich, J. K. Miller, W. M. Owen, B. G. Williams, D. K. Yeomans, J. D. Giorgini, D. W. Dunham, R. W. Farquhar, J. V. McAdams, and D. J. Scheeres, "Preliminary Considerations for NEAR's Low-Altitude Passes and Landing Operations at 433 Eros," AIAA Paper 98-4397, 1998 AIAA/AAS Astrodynamics Specialist Conference, Boston, Massachusetts, August 10–12, 1998.

[2] D. Brouwer and G. M. Clemence, *Methods of Celestial Mechanics*, New York: Academic Press, 1961.

[3] A. F. Cheng, O. Barnouin-Jha, M. T. Zuber, J. Veverka, D. E. Smith, G. A. Neumann, M. Robinson, P. Thomas, J. B. Garvin, S. Murchie, C. Chapman, and L. Prockter, "Laser Altimetry of Small-Scale Features on 433 Eros from NEAR-Shoemaker," *Science,* vol. 292, pp. 488–491, 2001.

[4] W. M. Kaula, *Theory of Satellite Geodesy,* Mineola, New York: Dover, 2000.

[5] M. Lara and D. J. Scheeres, "Stability Bounds for Three-Dimensional Motion Close to Asteroids," AAS Paper 02-108 presented at the 2002 AAS/AIAA Space Flight Mechanics Meeting, San Antonio, Texas, January 2002.

[6] C. Marchal, *The Three Body Problem,* New York: Elsevier, 1989.

[7] J. K. Miller, W. E. Bollman, R. P. Davis, C. E. Helfrich, D. J. Scheeres, S. P. Synnott, T. C. Wang, B. Williams, and D. K. Yeomans, "Navigation Analysis for Eros Rendezvous and Orbital Phases," *Journal of the Astronautical Sciences*, vol. 43, pp. 453–476, 1995.

[8] J. K. Miller, A. S. Konopliv, P. G. Antreasian, J. J. Bordi, S. Chesley, C. E. Helfrich, W. M. Owen, D. J. Scheeres, T. C. Wang, B. G. Williams, and D. K. Yeomans, "Determination of Shape, Gravity, and Rotational State of Asteroid 433 Eros," *Icarus* vol. 155, pp. 3–17, 2002.

[9] D. J. Scheeres, S. J. Ostro, R. S. Hudson, and R. A. Werner, "Orbits Close to Asteroid 4769 Castalia," *Icarus*, vol. 121, pp. 67–87, 1996.

[10] D. J. Scheeres, "The Effect of C_{22} on Orbit Energy and Angular Momentum," *Celestial Mechanics and Dynamical Astronomy,* vol. 73, pp. 339–348, 1999.

[11] D. J. Scheeres and F. Marzari, "Spacecraft Dynamics Far from a Comet," *Journal of the Astronautical Sciences,* vol. 50, no. 1, pp. 35–52, 2002.

[12] D. J. Scheeres, B. G. Williams, and J. K. Miller, "Evaluation of the Dynamic Environment of an Asteroid: Applications to 433 Eros," *Journal of Guidance, Control, and Dynamics,* vol. 23, no. 3, pp. 466–475, 2000.

[13] D. J. Scheeres, "Changes in Rotational Angular Momentum due to Gravitational Interactions between Two Finite Bodies," *Celestial Mechanics and Dynamical Astronomy*, vol. 81, pp. 39–44, 2001.

[14] D. J. Scheeres, "Design and Analysis of Landing and Low-Altitude Asteroid Flyovers," AAS Paper 01-138 presented at the 2001 AAS/AIAA Spaceflight Mechanics Meeting, Santa Barbara, California, February 2001.

[15] B. Villac, D. J. Scheeres, L. A. D'Amario, and M. D. Guman, "The Effect of Tidal Forces on Orbit Transfers," AAS Paper 01-247 presented at the 2001 AAS/AIAA Spaceflight Mechanics Meeting, Santa Barbara, California, February 2001.

[16] R. A. Werner and D. J. Scheeres, "Exterior Gravitation of a Polyhedron Derived and Compared with Harmonic and Mascon Gravitation Representations of Asteroid 4769 Castalia," *Celestial Mechanics and Dynamical Astronomy,* vol. 65, pp. 313–344, 1997.

[17] D. K. Yeomans, P. G. Antreasian, J.-P. Barriot, S. R. Chesley, D. W. Dunham, R. W. Farquhar, J. D. Giorgini, C. L. Helfrich, A. S. Konopliv, J. V. McAdams, J. K. Miller, W. M. Owen, Jr., D. J. Scheeres, P. C. Thomas, J. Veverka, and B. G. Williams, "Radio Science Results During the NEAR-Shoemaker Spacecraft Rendezvous with Eros," *Science,* vol. 289, pp. 2085–2088, 2000.